HHS Public Access

Author manuscript

Arthritis Rheumatol. Author manuscript; available in PMC 2016 May 01.

Published in final edited form as:

Arthritis Rheumatol. 2016 May ; 68(5): 1233–1244. doi:10.1002/art.39535.

Development of Th17-associated interstitial kidney inflammation in lupus-prone mice lacking the gene encoding Signal Transduction and Activator of Transcription-1 (STAT-1)

Gloria Yiu[1], **Tue Kruse Rasmussen**[1,2], **Bahareh Ajami**[3], **David J. Haddon**[1], **Alvina D. Chu**[1], **Stephanie Tangsombatvisit**[1], **Winston A. Haynes**[1], **Vivian Diep**[1], **Larry Steinman**[3,5], **James Faix**[4], and **Paul J. Utz**[1,5]

[1]Department of Medicine, Division of Immunology and Rheumatology, Stanford University School of Medicine, Stanford, California, USA

[2]Department of Biomedicine, Aarhus University, 8000 Aarhus C, Denmark

[3]Department of Neurology, Stanford University School of Medicine, Stanford, California, USA

[4]Department of Pathology, Stanford University School of Medicine, Stanford, California, USA

[5]Institute for Immunity, Transplantation, and Infection

Abstract

Type I interferon (IFN-I) signaling is a central pathogenic pathway in Systemic Lupus Erythematosus (SLE), and therapeutics targeting IFN-I signaling are in development. Multiple proteins with overlapping function participate in IFN signaling, but the signaling events downstream of receptor engagement are unclear. We employed highly-multiplexed assays to characterize autoantibody production, cytokine/chemokine profiles, and Signal Transduction and Activators of Transcription (STAT) phosphorylation to investigate the individual roles of IFNAR2, IRF9 and STAT1 in MRL/*lpr* (*lpr*) mice. Surprisingly, we found that *Stat1*$^{-/-}$, but not *Irf9*$^{-/-}$ or *Ifnar2*$^{-/-}$ mice, developed interstitial nephritis characterized by infiltration with RORγT^{+} lymphocytes, macrophages and eosinophils. Despite pronounced interstitial kidney disease and abnormal kidney function, *Stat1*$^{-/-}$ mice had decreased proteinuria, glomerulonephritis and autoantibody production. Phospho-specific flow cytometry (phosphoflow) revealed shunting of STAT phosphorylation from STAT1 to STAT3/4. In summary, we describe unique contributions of

Corresponding author: Paul J Utz, Professor of Medicine, Department of Medicine, Division of Immunology and Rheumatology, Stanford University – School of Medicine, CCSR Building, Room 2215A, 269 Campus Drive, Stanford, CA 94305. pjutz@stanford.edu. Phone: 650 724-5321.
(GY) Gloria Yiu, PhD, MD student.
(TKR) Tue Kruse Rasmussen, MD, PhD.
(BAJ) Bahareh Ajami, PhD.
(DJH) David J. Haddon, PhD.
(ADC) Alvina D. Chu, MD.
(ST) Stephanie Tangsombatvisit, MD student.
(WAH) Winston A. Haynes, PhD student.
(VKD) Vivian Diep, Research assistant.
(LS) Larry Steinman, MD, Prof.
(JF) James Faix, MD, Prof.
(PJU) Paul J. Utz, MD, Prof.

Conflict of interest: We declare that no conflicts of interest exist.

STAT1 to pathology in different kidney compartments, and provide novel insight into tubulointerstitial nephritis (TIN) a poorly understood complication that predicts end-stage kidney disease in SLE patients.

Keywords

MRL/*lpr*; IFNAR2; IRF9; STAT1; interferon signaling; SLE; Th17; interstitial nephritis

INTRODUCTION

Systemic Lupus Erythematosus (SLE) is a chronic autoimmune disease characterized by inflammatory destruction of multiple organs, including the skin, vasculature, and kidneys. Patients are treated with glucocorticoids, NSAIDs, cytotoxic agents, hydroxychloroquine, mycophenolate mofetil (MMF) and Rituximab, alone or in combination[1]. In the last decade, pathophysiological pathways in SLE have been discovered and targeted. These include therapies targeting B cell activator factor (BAFF) and IFNα (a Type I interferon, IFN-I) [2].

Evidence that IFNα plays a crucial role in SLE is extensive. A subset of patients administered IFNα for hepatitis or malignancies develop a SLE-like illness, ranging from development of anti-nuclear antibodies (ANA) to frank autoimmunity meeting SLE diagnostic criteria[3]. These data show that sustained exposure to high levels of IFNα can induce an SLE-like syndrome. Transcript profiling of bulk peripheral blood mononuclear cells (PBMCs) and immune cell subsets from SLE patients demonstrated the presence of an IFNα-inducible gene expression signature or “IFN biosignature” in over half of SLE patients[4,5]. The IFN biosignature has been shown to correlate with Systemic Lupus Erythematosus Disease Activity Index (SLEDAI) and the American College of Rheumatology (ACR) 1997 revised SLE criteria[6]. Using the IFN biosignature, patients can be stratified as IFN-high or IFN-low patients.

The IFN biosignature has been robustly recapitulated in murine models of SLE that serve as powerful tools in elucidating the role of pleotropic proteins like IFNα[7]. However, results from groups studying lupus-prone mice lacking the α- chain of IFN-α/βR (called *IFNAR1*) are inconsistent, reporting either improved or worsened disease in mice of differing genetic backgrounds[8–10]. Our group has previously defined important roles for IFNAR2, Interferon Regulatory Factor 9 (IRF9), and Signal Transduction and Activator of Transcription 1 (STAT1, Supplemental Fig. S1) in the pristane murine model[11,12]. We identified defects in Toll-like receptor (TLR)-7/9 specific B cell responses and isotype-switched IgG autoantibodies in *Ifnar2*$^{-/-}$, *Irf9*$^{-/-}$ and *Stat1*$^{-/-}$ mice. These results support a model where IFN signaling is upstream of TLR-specific B cell responses, and is important for the production of isotype-switched IgG autoantibodies.

Because the pristane model is an inducible model associated with mild kidney pathology, the role of IFNAR2, IRF9, and STAT1 in spontaneous development of organ-specific involvement such as glomerulonephritis (GN) is unclear. In the *lpr* model, SLE-like pathogenesis results from a loss-of-function mutation in the *Fas* gene (lymphoproliferation, *lpr*), which leads to defects in negative selection of autoreactive B and T lymphocytes. *Lpr*

mice recapitulate many human SLE pathologies – particularly progressive immune-complex mediated GN seen in lupus nephritis, a leading cause of mortality[13,14]. Other features include female bias; diffuse organ inflammation; and autoantibodies directed against DNA and RNA containing antigens[15].

Given the plethora of cytokines that are dysregulated in the promotion of autoimmunity[16–18], growing interest has centered on shared signaling pathways including phosphorylation of STAT family members. Cytosolic STATs are activated through receptor ligation and subsequent tyrosine phosphorylation by Janus family tyrosine kinases (JAKs). This results in translocation of STATs to the nucleus and initiation of transcription of many genes, including those vital to immune function[19].

Here we investigate the individual contributions of the IFN-I/II signaling components IFNAR2, IRF9 and STAT1 to spontaneous SLE pathogenesis in the *lpr* mouse model. Employing high-throughput methods for characterizing autoantibody profiles and JAK-STAT signaling pathways, we investigate how disease manifestations are impacted by loss of the genes encoding each individual protein. Unexpectedly, we discovered that STAT1 plays a central role in the development of interstitial nephritis mimicking tubulointerstitial nephritis (TIN), which correlates with end-stage renal failure in SLE patients[20]. We further demonstrate marked infiltration of the kidney interstitium with Th17 lymphocytes; enrichment of Th17 cells in secondary lymphoid organs; alterations in autoantibody profiles; elevated levels of cytokines, chemokines and growth factors; and shunting of STAT1 signaling to other cytokine pathways. Taken together, our results suggest that pharmacological inhibition of STAT1 leads to ameliorated glomerular disease, but may cause tubulointerstitial pathology and other unanticipated effects on the immune system.

RESULTS

IFN-I/II knockout (KO) mice exhibit decreased proteinuria while *Stat1*$^{-/-}$ mice have elevated renal function markers

A hallmark of human and murine SLE is the development of GN, in which immune complex deposition in glomeruli results in inflammation and failure to retain proteins[21,22]. We hypothesized that mice with defects in IFN signaling would have less severe inflammation and thus would be protected from GN development. We assessed proteinuria in *Ifnar2*$^{-/-}$, *Irf9*$^{-/-}$, *Stat1*$^{-/-}$, *lpr* and MRL/*mpj* (*mpj*) female mice at 16 weeks to allow for disease development in organ systems including the kidneys[23–26]. *Mpj* mice lack the *lpr* mutation and served as a control strain. As expected, *lpr* mice developed significantly higher levels of proteinuria compared to *mpj* controls ($p<0.001$, Fig. 1a). Mice lacking IFNAR2, IRF9 *or* STAT1 all exhibited significantly decreased proteinuria compared to *lpr mice* ($p<0.05$; $p<0.0001$; $p<0.0001$, respectively), indicating relatively preserved glomerular function, consistent with our initial hypothesis.

IFNAR2 and IRF9 ablation led to decreased serum levels of both creatinine and blood urea nitrogen (BUN) as compared to *lpr* mice, although not statistically significant (Fig. 1b–c). As expected, *lpr* mice had significantly higher serum levels of both creatinine and blood urea nitrogen (BUN) as compared to *mpj* mice ($p<0.01$). Surprisingly, *Stat1*$^{-/-}$ mice also

exhibited increased creatinine and BUN levels as compared to *mpj* mice, suggesting poor renal function despite improved proteinuria (p=0.01 and p=0.03).

Stat1$^{-/-}$ mice develop unexpected interstitial kidney disease

Kidney disease in SLE patients can be categorized into distinctive classes in which different areas of the kidney are affected. Because proteinuria is largely a measure of glomerular damage, further studies were performed to assess global kidney morphology. We performed Periodic Acid-Schiff (PAS) staining on sections prepared from paraffin-embedded kidneys (Fig. 2a) and quantified renal nephritis using the NIH Activity and Chronicity Indices in a blinded manner[27] (Supplemental Table S1).

As we predicted, *Irf9*$^{-/-}$ and *Stat1*$^{-/-}$ mice exhibited lower acute and chronic glomeruli scores compared to *lpr* mice, although this result was not statistically significant (Fig. 2b–e). Conversely, *Ifnar2*$^{-/-}$ kidneys had increased acute and chronic glomerular scores as compared to *lpr* kidneys, although this also was not statistically significant. Unexpectedly, *Stat1*$^{-/-}$ kidneys showed significantly increased acute and chronic tubulointerstitial pathology compared to *lpr* kidneys (p=0.0007 and p=0.0002, respectively, Fig. 2d–e), which was not observed in *Ifnar2*$^{-/-}$, *Irf9*$^{-/-}$, and *mpj* kidneys. To further investigate this finding, we performed immuno-histochemical stains on kidney sections for the leukocyte marker CD45 (Fig. 2a). We observed marked interstitial infiltration of CD45^{+} leukocytes in kidneys from *Stat1*$^{-/-}$ mice as compared to *Ifnar2*$^{-/-}$, *Irf9*$^{-/-}$, *lpr* and *mpj* mice, suggesting an immune cell-mediated process was responsible for the tubolointerstitial disease.

RORγT^{+} cells infiltrate the interstitium of *Stat1*$^{-/-}$ mice

Glomerulonephritis observed in *lpr* mice is a B cell-associated process characterized by deposition of IgM, IgG, and complement component C3 (C3)[21,22]. Recently, elevated levels of Th17 lymphocytes – a subset of inflammatory T cells – has also been described in both the peripheral blood and kidneys of lupus nephritis patients[28–30]. To better characterize the immune cell infiltrate within the interstitium of KO mice, we performed a series of immunohistochemical stains. In addition to stains characterizing GN, we performed stains for RORγT (the canonical transcription factor required for Th17 cell development), IBA1 (a macrophage marker) and eosinophils. Both macrohpages[31] and eosinophils[32–34] have been described in polarization and downstream function of Th17 lymphocytes.

As expected, *lpr* kidneys showed increased IgM and IgG deposition in the glomeruli as compared to kidneys from BALB/c mice (Fig. 3a). In contrast, minimal staining for IgM and IgG was observed in the glomeruli of *Stat1*$^{-/-}$ mice, suggesting that other factors and/or cell types are involved. We observed impressive infiltration of RORγT^{+} cells confined to the interstitium of *Stat1*$^{-/-}$ mice (Fig. 3a, right). *Stat1*$^{-/-}$ interstitium also demonstrates increased staining for IBA1 (Fig. 3a, right) and eosinophils on hemotaxylin-eosin (H&E) stain (Supplemental Fig. S2). Taken together, histologic evaluation of kidney specimens implicates a role for RORγT^{+} cells in mice lacking STAT1, in contrast with the central role played by B lymphocytes in *lpr* mice with GN.

Th1/Th17 polarization is altered in IFN-I/II signaling KO mice

In addition to their role in kidney disease, the circulating Th17 cell population is increased in SLE patients[35]. We hypothesized that ablation of STAT1 would lead to increased Th17 polarization in secondary lymphoid organs. To test this hypothesis, we quantified the proportions of IL-17A and IFNγ producing lymphocytes in the spleen and lymph nodes (axillary, mandibular and mesenteric) of *Ifnar2*$^{-/-}$, *Irf9*$^{-/-}$, *Stat1*$^{-/-}$, and *lpr* mice by flow cytometry.

The proportion of IL-17A^{+} CD4^{+} T cells was increased in *Stat1*$^{-/-}$ splenocytes by more than eight fold compared to *lpr* splenocytes (0.84% vs 0.10%, respectively) (Fig. 3b) and was significantly increased across multiple mice (p=0.007, Fig. 3c). No significant changes were observed in the frequencies of IL-17A producing CD4^{+} T cells in *Ifnar2*$^{-/-}$ and *Irf9*$^{-/-}$ (0.15% and 0.04%, respectively) as compared to *lpr* mice (Fig. 3b). To test whether absence of STAT1 alone would lead to expansion of the Th17 lymphocyte population, intracellular cytokine staining (ICS) of IL-17A was also performed on BALB/c splenocytes lacking STAT1. No significant enrichment was found when compared to wildtype BALB/c mice (Supplemental Fig. S3).

As expected, fewer IFNγ-producing CD4^{+} T cells were observed in spleen and lymph nodes obtained from *Stat1*$^{-/-}$ mice as compared to cells obtained from *lpr* mice (12.12% and 30.02% from spleen, respectively) (Fig. 3b) and was significantly decreased across multiple mice (Fig. 3d, p=0.004). *Ifnar2*$^{-/-}$ and *Irf9*$^{-/-}$ mice had significantly larger populations of IFNγ-producing CD4^{+} T cells in both spleens and lymph nodes (42.56% and 53.6% from spleen, respectively) (Fig. 3b), also significant across multiple mice (p=0.0185, Fig. 3d). These results suggest that crosstalk between IFN-I and IFN-II signaling occurs where in the absence of IFN-I signaling proteins, a compensatory increase in IFNγ signaling is observed, likely mediated by STAT1 which is shunted from IFN-I to IFN-II signaling.

Stat1$^{-/-}$ mice exhibit decreased IgM/G autoantibody production against SLE-associated antigens

Antibodies directed against autoantigens are clinically relevant in GN[36], while the role of autoantibodies in interstitial kidney disease is not well understood. We employed protein microarrays to profile autoantibodies in the sera of *Stat1*$^{-/-}$, *Ifnar2*$^{-/-}$, *Irf9*$^{-/-}$, and *lpr* mice. This method has been well-established by our lab for studying human[37–42] and murine SLE[11,12,43]. In brief, arrays containing over 600 features and comprised of more than 100 unique proteins and peptides that are known or putative SLE autoantigens were printed, probed with sera derived from knockout mice and bound autoantibodies were detected with a fluorophore-conjugated secondary antibody. Arrays were scanned, and fluorescence intensity was quantitated. The Significance Analysis of Microarrays (SAM) algorithm[44] was then employed to determine antigens with statistically significant differences between groups of mice, and a hierarchical clustering program grouped individual mice based on similar autoantibody profiles.

IgM autoantibody reactivity against SLE-associated autoantigens was decreased in *Stat1*$^{-/-}$ as compared to *lpr* mice (Fig. 4a). SAM identified 12 of these IgM autoantibodies as

significantly decreased in *Stat1*$^{-/-}$ sera compared to *lpr* sera. Differentially-targeted autoantigens included U1-snRNP, histones, dsDNA, CENP-B, and PM/Scl75, many of which are important in human SLE. SAM identified a similar but constricted subset of IgG autoantibodies that were significantly decreased in *Stat1*$^{-/-}$ compared to *lpr* sera (Fig. 4b).

When comparing *Irf9*$^{-/-}$ and *lpr* sera, SAM identified increased IgM and IgG autoantibody reactivity against histones in *Irf9*$^{-/-}$ sera (Supplemental Fig. S4a and S4b). These data reveal a potentially unique role for IRF9 in antibody production against histones. We did not identify any antigens with significantly different reactivity when comparing *Ifnar2*$^{-/-}$ and *lpr* sera. All significant array findings were validated using enzyme-linked immunosorbent assay (ELISA). Of 22 SAM-identified antigens identified in the entire study across all strains, 17 were confirmed by ELISA to have significant differences in titer between KO and *lpr* mice (Fig. 4c, and Supplemental Figs. S4c and S5).

STAT1 is required for the expression and upregulation of TLR7 by IFNα

Nucleic acid components of SLE autoantigens can activate autoreactive B cells via TLR7, which recognizes RNA, and TLR9, which recognizes DNA. TLR expression is also upregulated by IFN-I secreted by pDCs in human naive B cells and modulates isotype switching[45]. We have previously demonstrated in the pristane model that mice lacking IFNAR2, IRF9 or STAT1 had defects in upregulating transcripts encoding TLR7 and/or TLR9 in response to IFNα exposure or TLR agonists[11,12]. Moreover, *Stat1*$^{-/-}$ pristane mice had a marked defect in isotype switching of autoantigen-specific B cells, but not B cells immunized with ovalbumin. We hypothesized that the decreased autoantibody production observed in *Stat1*$^{-/-}$ *lpr* mice was due to a similar defect in TLR7/9 upregulation.

Splenic B cells were obtained from *Stat1*$^{-/-}$ and *lpr* mice, cultured in the presence or absence of IFNα, and relative mRNA expression levels of TLR7, TLR9 and Mx1 (a known IFNα-inducible gene) normalized to β2M and GAPDH were determined by realtime quantitative PCR. The expression of TLR7, but not TLR9, was significantly upregulated in IFNα-treated B cells from *lpr* mice, but this upregulation was almost completely abolished in *Stat1*$^{-/-}$ B cells (Fig. 4d, left). Therefore, STAT1 is required for IFNα-inducible expression of TLR7 but not TLR9 in murine B cells. Because *Stat1*$^{-/-}$ mice have decreased reactivity against both DNA- and RNA-associated antigens, these data suggest overlap of RNA/DNA-sensing by TLR7/9, perhaps through differential endosomal trafficking in the absence of STAT1[46]. Alternatively, it is possible that defects in autoantibody production in *Stat1*$^{-/-}$ mice result from TLR-independent pathways.

As expected, induction of expression of Mx1 mRNA was significantly decreased in B cells from *Stat1*$^{-/-}$ mice ($p=0.016$, Fig. 4e) compared to *lpr* B cells. However, *Stat1*$^{-/-}$ B cells stimulated with IFNα retain the ability to significantly upregulate Mx1 expression as compared to unstimulated cells ($p=0.02$, Fig. 4e), revealing that STAT1 is dispensable for IFNα signaling. This finding supports work demonstrating high redundancy and plasticity of STAT phosphorylation in different physiological states[47,48]. We tested the hypothesis that IFNα signaling can signal through molecules other than STAT1 using phosphoflow cytometry.

Disruption of genes encoding IFN-I/II signaling proteins results in shunt STAT phosphorylation to different cytokine signaling pathways

In addition to the finding that SLE patients have abnormal levels of many serum cytokines and chemokines, many of which are interferon inducible, several publications have demonstrated that dysregulated STAT signaling plays a role in murine models of SLE and in human SLE patients[49,50]. We hypothesized that both Th1/Th17 polarization (Fig. 3b-3d) and transcription events downstream of IFNα signaling (Fig. 4d-4e), observed in the absence of IFN-I/II signaling proteins could be attributed to dysregulated STAT signaling.

Splenocytes from individual mice were isolated and stimulated with individual cytokines for 20 minutes. We then used phosphoflow cytometry to measure phosphorylation of STATs 1, 3, 4, 5, and 6 in $CD4^+$ T cells ($CD3^+CD4^+CD8^-$), $CD8^+$ T cells ($CD3^+CD4^-CD8^+$), and B cells ($CD3^-CD4^-CD19^+$) from *Stat*$1^{-/-}$, *Ifnar2*$^{-/-}$, *Irf9*$^{-/-}$, and *lpr* mice. We selected cytokines thought to play critical roles in SLE pathogenesis including IFNα, IFNγ, IL-21, and IL-27[51–53]. To identify additional cytokines to include in the stimulation panel, we performed a multiplex bead-based assay on *Stat*$1^{-/-}$, *Ifnar2*$^{-/-}$, *Irf9*$^{-/-}$, and *lpr* serum to determine levels of 26 different cytokines and chemokines (Supplemental Fig. S6). Compared to *lpr* sera, sera from *Stat*$1^{-/-}$ mice had significantly increased levels of TNFα, IL-4 and eotaxin, in addition to significantly decreased levels of IL-12p40, a cytokine that is critical for Th1 polarization[54,55]. *Irf9*$^{-/-}$ sera also had significantly increased levels of IL-4, as well as IL-1a when compared to *lpr* sera. Based on these findings, IL-4 and IL-12 were added to our stimulation panel.

Phosphoflow profiling resulted in 1,980 data nodes, where each node represents phosphorylation levels of an individual STAT protein, in response to a single stimulation in a unique cell subset. As expected, *Stat*$1^{-/-}$ mice had no STAT1 phosphorylation across all cell subsets (Fig. 5a). In response to IFNα, STAT3 phosphorylation was significantly increased in all subsets of *Stat*$1^{-/-}$ mice compared to *lpr* mice (Supplemental Fig. S7). IFNα stimulation also resulted in significantly increased STAT4 phosphorylation both in $CD4^+$ and $CD8^+$ T cells of *Stat*$1^{-/-}$ compared to *lpr* mice. These data strongly suggest that IFNα can signal through STAT3/4 and potentially other factors.

Irf9$^{-/-}$ mice had increased STAT3 phosphorylation in $CD8^+$ T cells as well as in $CD19^+$ B cells after IFNα stimulation. Significantly increased STAT4 phosphorylation was observed in $CD4^+$ and $CD8^+$ T cells from *Irf9*$^{-/-}$ mice in response to IFNγ stimulation compared to *lpr* T cells (Supplemental Fig. S8). This result may explain our finding that *Irf9*$^{-/-}$ mice have higher frequencies of IFNγ producing $CD4^+$ T cells (Fig. 3b and 3d), as increased signaling in response to IFNγ exposure may be part of a positive feedback loop that drives the development of IFNγ-secreting T cells.

All cell subsets in *Ifnar2*$^{-/-}$ mice compared to *lpr* mice exhibited significantly reduced phosphorylation of STAT1, 3, 4, and 5 in response to IFNα stimulation (Supplemental Fig. S9). These results support a model where the IFNAR2 component of the IFNAR dimeric receptor complex is necessary for receptor signaling. Interestingly, enhanced phosphorylation of STAT5 in response to IL-27 was significantly and consistently observed both in $CD4^+$ and $CD8^+$ T cells of *Ifnar2*$^{-/-}$ mice compared to *lpr* mice. This result shows

that in the absence of IFNAR2, IL-27 signaling can be modulated from phosphorylation of STAT1/3 to phosphorylation of STAT5. It serves as additional evidence of STAT redundancy in different biological states.

DISCUSSION

Using highly multiplexed analyses we show how loss of individual IFN-I/II signaling molecules IFNAR2, IRF9, and STAT1 affects renal disease, autoantibody profiles, T cell subsets, and cytokine signal transduction. Notably, genetic deletion of STAT1 leads to decreased autoantibody production and GN, but induces severe interstitial inflammation accompanied by infiltration of RORγT^{+} cells, CD45^{+} leukocytes, macrophages, and eosinophils in the interstitium. STAT1 ablation results in altered signal transduction characterized by shunting to alternative STAT molecules including STAT3, a key transcription factor involved in Th17 cell differentiation. Together, our findings demonstrate a critical role for STAT1 in the development of Th17 associated autoimmune interstitial kidney disease in a murine model of SLE.

Prevention and treatment of kidney disease is crucial for clinicians who care for SLE patients. Despite a reported prevalence of TIN in SLE kidney biopsies ranging from 23% by Park *et al.*[56] up to 72% by Hsieh *et al.*[20], very little is known regarding the immunologic mechanisms underlying TIN. Most histologic measures focus on glomerular involvement to inform therapeutic decisions, but have suboptimal predictive value in renal outcomes. In contrast, multiple groups have shown that SLE patients with TIN are at greatest risk of renal failure as defined by initiation of chronic dialysis treatment or requirement for renal transplant[20,57]. Our results lend support to this model as only *Stat1*$^{-/-}$ mice with predominant TIN, and not *Ifnar2*$^{-/-}$, *Irf9*$^{-/-}$ or *lpr* mice with predominant GN, showed elevation in kidney markers BUN and creatinine. These results suggest that TIN, more so than GN, contributes to decreased renal function.

IL-17A is thought to play an important role in SLE pathogenesis[58–60]. The proportion of Th17 cells in blood of SLE patients is elevated and correlates with SLEDAI and with the presence of lupus nephritis[61,60]. IL-17 levels are also elevated in SLE sera[62]. Organ-specific expression of IL-17A-producing cells, particularly in the kidney, is more controversial. Wang *et al.* employed single cell laser capture microdissection to study cytokine expression levels in glomeruli versus interstitium and observed increased IL-17A mRNA expression both in cells isolated from glomeruli and interstitium of SLE patients. They were unable to detect IL-17A in kidneys by immune-histochemical staining in contrast to Crispin *et al.* who successfully detected IL-17A by similar staining methods[63].

Because staining for IL-17A in murine systems has been difficult and results are controversial, we instead focused on the transcription factor RORγT, a canonical regulator of Th17 cell differentiation. We demonstrated RORγT staining in renal interstitium with concurrent staining of IBA1 in *Stat1*$^{-/-}$ but not in *lpr* mice. FACS analysis demonstrated significantly higher proportions of Th17 cells in lymph nodes and splenocytes derived from *Stat1*$^{-/-}$ mice as compared to *lpr* mice. These data robustly support a role for STAT1 in inhibiting Th17 lymphocyte polarization and trafficking to kidney interstitium in *lpr* mice.

Costaining of eosinophils with RORγT^{+} cells in the interstitium of *Stat1*$^{-/-}$ as compared to *lpr* mice further supports Th17 lymphocyte activity as IL-17A upregulates various cytokines that promote eosinophillic inflammation[32–34]. Multiplexed cytokine profiling studies also revealed increased levels of serum eotaxin, an eosinophil chemotactic chemokine, in *Stat1*$^{-/-}$ as compared to *lpr* mice. Taken together, these data support our hypothesis that interferon signaling plays a role in Th17 cell differentiation and SLE pathology, and that STAT1 in particular plays a central role in Th17-associated TIN.

Despite our findings, our study is limited by the inability to dissect potential independent effects of STAT1 ablation on immune and renal parenchyma cells. Previous work has described elevated levels of IFNγ mRNA in *lpr* renal cells themselves[64,65], resulting in the increased production of inflammatory cytokines like CSF-1 and TNF-α which can induce apoptosis of tubular epithelial cells involved in interstitial homeostasis[66]. Our finding of severe Th17-associated tubulointerstitial disease is unexpected in the setting of STAT1 ablation since IFNγ signaling requires STAT1 homodimerization and translocation to the nucleus where it binds to gamma activated site (GAS)-containing genes. Adoptive transfer of *Stat1*$^{-/-}$ hematopoietic stem cells (HSCs) or IL-17 producing cells into *lpr* mice was unsuccessful due to difficulty with breeding and radiosensitivity of the *lpr* background strain. Further experiments are planned to shed light on the independent role of STAT1 in renal versus hematopoietic cells.

It should be noted that disease severity in our mouse colony was observed to be less pronounced than other published studies, but does not affect the conclusions we have reached. Several possibilities exist for this discrepancy. Variability in disease development within strains housed in different facilities has been reported. Factors such as diet, sex of handler, and site of blood collection (retro-orbital, vena cava or tail vein) can impact both behavioral and physiologic readouts[55–57,67–69]. Finally, nephritis development is dependent on age at analysis. Previous studies have euthanized mice at 20 – 24 weeks where disease severity and mortality is high. In accordance with guidelines of the Institutional Animal Care and Use Committee of Stanford University, euthanasia of 16-week-old mice was recommended as it allowed for both full development of disease manifestations and humane care.

Analysis of cytokine production and STAT phosphorylation in *Stat1*$^{-/-}$ splenocytes allowed us to investigate signaling mechanisms that could in part help to explain differences observed in T-helper cell polarization. We hypothesized that Th17 cell enrichment was associated with compensatory STAT3/4 phosphorylation, both previously described in Th17 cell polarization[70–72]. Our phosphoflow profiling data support this hypothesis as *Stat1*$^{-/-}$ splenocytes exhibited shunted phosphorylation to STAT3/4 downstream of multiple stimuli including IFNα, IL-21 and IL-27, and across multiple cell subsets. Phosphorylation of other STAT proteins in response to IFNα supports our qPCR data showing that *Stat1*$^{-/-}$ B cells retain the capacity to upregulate the transcription of the interferon-inducible gene *Mx1* upon IFNα receptor ligation, presumably mediated by STAT3/4.

Phosphoflow analysis of cells from *Ifnar2*$^{-/-}$ mice shows little if any STAT phosphorylation upon IFNα stimulation. Despite lack of IFNα signaling, *Ifnar2*$^{-/-}$ mice still have prominent

autoantibody production and moreover have marginally increased kidney pathology, both of which have previously been associated with high IFN signaling rather than absence of IFN signaling[6,7]. One potential explanation for the discrepancy between phenotypes of *Ifnar2*$^{-/-}$ and *Stat1*$^{-/-}$ mice is that *lpr* pathology is driven by IFNγ, which requires STAT1 for signal transduction through its receptor, and that IFNα is less influential[65]. However, evidence shows that both IFNα and IFNγ can induce the formation of the IFN-stimulated gene factor 3 (ISGF3) complex and bind to IFN-stimulated Response Element (ISRE) and gamma activated site (GAS)-containing genes, repectively[73,74]. IFNα- and IFNγ-inducible genes have ~25% overlap, and genes most highly upregulated by IFNα are also IFNγ-inducible[75].

Differences exist between the biology of IFN-I and IFN-II signaling proteins. IFNAR1/2 have both been shown to either directly or indirectly interact with other proteins including TAM family members, which are thought to inhibit IFN-I-induced inflammation[76]. It is possible that loss of IFNAR2 inhibits both anti-inflammatory TAM signaling in addition to inflammatory IFN signaling, resulting in a net-neutral effect. Treatment of *lpr* mice with a monoclonal anti-IFNAR antibody ameliorates disease at early time points. At later stages of disease, IFN-I signaling-independent pathways overcome the therapeutic effects[77]. Mangini *et al* posit that one of these pathways is downstream of IFNγ, suggesting important interactions between IFN-I/II signaling pathways. We demonstrate direct evidence of crosstalk with increased IFNγ production in the secondary lymphoid organs of *Ifnar2*$^{-/-}$ and *Irf9*$^{-/-}$ mice. Crosstalk is likely attributed to shared phosphorylation of STAT1 downstream of IFNα and IFNγ in addition to promiscuity of STAT phosphorylation.

Our studies highlight the complexity of IFN-I/II signaling and the necessity for mechanistic studies in implementing therapies targeting IFNs and JAK-STATs. Our *Stat1*$^{-/-}$ model of Th17-associated TIN may lead to better understanding of JAK-STAT inhibitors like Tofacitinib, which inhibits JAK1/3[78]. While there are no reports of Tofacitinib-induced TIN, no murine studies have addressed the effects of JAK1/3 inhibition on autoimmune renal diseases. IFN-targeted therapies Sifalimumab (MEDI-545) and Rontalizumab (RG7415) are still in early-stage clinical trials, and suggest that IFN inhibitors may be beneficial in certain subsets of patients[79–81]. Our results underscore the potential benefits in subsetting disease not only on IFNα signaling but also signaling of other cytokines like IFNγ and IL-21. Future human studies will benefit from proteomic analysis to understand global cytokine signaling in patients to guide trial design and to characterize mechanistic effects of targeted therapies. Taken together, the present study reveals unique contributions of IFN signaling proteins to SLE pathogenesis and highlights a role for STAT1 in interstitial kidney disease in SLE. These results have the potential to improve our understanding of clinically important TIN and to guide studies of targeted cytokine therapies in patients.

METHODS

Mice

Ifnar2$^{-/-}$ mice on the BALB/c background were kindly provided by Paul J Hertzog (Monash University, Clayton, Australia). *Irf9*$^{-/-}$ mice on the BALB/c background were purchased from RIKEN BioResearch Center. *Stat1*$^{-/-}$ mice on the BALB/c background were a generous gift from J. Durbin (Ohio State University, Columbus, Ohio, USA). All knockout

mice were backcrossed onto the *lpr* (Jackson Laboratories) background to the N8-N10 generation. Mice used in this study were maintained under standard conditions at the Stanford University Research Animal Facility. Data presented are from female mice euthanized at 16 weeks of age. Due to the characteristically small litter sizes and poor breeding behavior of *lpr* mice, the use of littermate wild type controls was not always possible. When breeding did not yield sufficient numbers of wild-type controls, age- and sex-matched *lpr* mice were substituted. All unique repeat experiments included both knockout and wild type mice. To ensure accuracy in breeding, every mouse analyzed in this study was genotyped for either homozygous ablation or presence of the desired gene (Supplemental Table T2). Proteinuria was monitored by dipstick analysis using Albustix (Bayer). Serum creatinine and BUN analysis was performed on Siemens Dimension Xpand analyzer. All animal experiments were approved by, and performed in compliance with, the guidelines of the Institutional Animal Care and Use Committee of Stanford University.

Histopathology and immunohistochemical staining

Mice were euthanized by CO_2 exposure followed by cervical dislocation. Kidneys were surgically removed, fixed in buffered formalin, embedded in paraffin, sectioned, and stained with either periodic acid-Schiff (PAS), Hemotaxylin and Eosin (H&E) or CD45 (30-F11, BD Pharmingen; performed by Histotec, Hayward, California, USA). The slides were scored in a blinded fashion by one of the authors (JF) according to NIH kidney scoring (Supplementary Table 1), both for acute and chronic disease indices.

Lupus autoantigen microarrays

Detailed autoantibody profiling protocols and a list of arrayed antigens have been previously published[39]. Briefly, SLE-associated autoantigens were printed at 0.2 mg/ml in ordered arrays on nitrocellulose-coated FAST slides (Whatman, Piscataway, New Jersey) using a VersArray ChipWriter Pro Robotic Arrayer (Bio-Rad). Individual arrays were blocked with PBS containing 3% FCS and 0.05% Tween 20 (Sigma-Aldrich) for 1.5 hrs on a rocking platform at room temperature. Arrays were probed with 400 µl mouse serum diluted 1:250 in 1X PBST with 5% FCS for 1.5 hrs on a rocking platform at 4°C, followed by washing and incubation with a 1:2000 dilution of cyanine-3-conjugated goat anti-mouse IgM or IgG secondary antibody (Jackson ImmunoResearch Laboratories). Arrays were scanned using a GenePix 4000B scanner (Molecular Devices) at constant PMT power for all arrays. The net mean pixel intensities of each feature were determined using GenePix Pro 6.1 software (Molecular Devices, Sunnyvale, California). Array data will be uploaded to the GEO database upon publication of the manuscript.

Enzyme-linked immunosorbent assays

96 well plates (NUNC MaxiSorp) were incubated at 4°C overnight with 100 µL/well protein solution at 2µg/ml (U1, His1000, H1, H2A, H2B, H3, dsDNA plasmid, dsDNA salmon sperm, dsDNA calf thymus, Intrinsic factor, MPO, Scl70, and CENPB). Plates were then washed 3X with phosphate buffered saline with 0.05% Tween 20 (PBST) and blocked with 200µL/well PBST with 5% FCS for 2 hrs at room temperature. After washing, plates were incubated with 100 µL/well of sample at three dilutions (1:400; 1:800; 1:1600) at 4°C overnight, followed by washing and development using Europium labeled anti-mouse IgG

and DELFIA Enhancement solution (PerkinElmer). For IgM autoantibody measurement, endogenous biotin was blocked in two steps by first incubating with streptavidin followed by biotin to block free binding sites on plate bound streptavidin. Samples were then incubated with DSB-X biotin goat anti-mouse IgM (Invitrogen), followed by washing with Europium labeled streptavidin, then developed using DELFIA enhancement solution. *Stat1*$^{-/-}$, n=5; *Irf9*$^{-/-}$, n=5, *lpr*, n=5, BALB/c, n=2. Detection limit was calculated as 2X the standard deviation of the blanks.

Real-time quantitative PCR

Splenocytes were harvested from *Irf9*$^{-/-}$ and *Stat1*$^{-/-}$, and *lpr* mice. B cells were negatively selected using magnetic beads (Miltenyi Biotech). Cells were more than 95% pure, as assessed by flow cytometry (CD19^{+}IgM^{+}biotin^{-}). B cells were cultured in RPMI supplemented with L-glutamine (2 mM), sodium pyruvate (1 mM), nonessential amino acids (0.1 mM), penicillin (100 U/ml), streptomycin (0.1 mg/ml), 2-ME (5×10^{-5} M), and FBS (10%) in the presence or absence of 1,000 IU/ml recombinant IFN-α (Calbiochem) for 4 hours. RNA was extracted using RNeasy Mini kit (Qiagen). RNA (10 ng) was amplified using 1-step QuantiTect SYBR Green RT-PCR (Qiagen) and 0.5 μM forward and reverse primers using an Opticon2 continuous fluorescence detector (MJ Research). The fold change in expression of each transcript normalized to β2M and GAPDH was determined by the $2^{-\Delta\Delta Ct}$ method. QuantiTect Primer Assay sets for murine TLR7, TLR9, MX1, B2M and GAPDH were purchased from Qiagen.

Immunofluorescence staining

Animals were injected intraperitoneally with ketamine (100 mg/kg) and diazepam (5 mg/kg) and monitored. Upon loss of nociceptive reflexes, animals were transcardially perfused with 30 mls of PBS/EDTA followed by 30 mls of 4% paraformaldehyde (wt/vol) in 0.1 M PBS at room temperature. Kidneys were removed and post-fixed in 4% paraformaldehyde at 4°C for up to 24 hrs then cryoprotected in 24% sucrose solution (wt/vol) in PBS for 24 hrs. Kidneys were embedded in Optimal Cutting Temperature compound (Tissue-Tek) and frozen at −80°C, then cut at 7-μm-sections. Sections were allowed to thaw at 20–24°C and rehydrated in PBS for 2 hrs then treated with 0.3% Triton in PBS for 30 mins. 300 ul of ice cold acetone was added to each section and place at −20 for 15 minutes. Immediately, wash with PBS three times. Blocking was performed with 5–10 μg ml^{-1} purified antibody to CD16/32 for 2 hrs. Primary antibody staining was performed overnight at 4°C for the following molecules: RORγT (AFKJS-9, eBioscience), Iba-1 (cat. #019–19741, Wako) and IgM (1020-01, SouthernBiotech). Secondary antibody staining was performed using donkey anti-goat Alexa Flour 647, donkey anti-rabbit Alexa Flour 568 or donkey anti-rat Alexa Flour 488 (Molecular Probes) in the dark for 1 hr at room temperature. All sections were analyzed by confocal microscopy using either a Leica SP2 AOBS Confocal Microscope or Leica SP8 Confocal Microscope. All images presented are maximum intensity projections of *z* stacks of individual optical sections.

Intracellular cytokine staining

Splenocytes and lymph nodes (axillary, submandibular, and mesenteric) were harvested in 4°C-chilled MACs buffer (PBS containing 1% FCS and 1 mM EDTA). Using the back of a

sterile 5 ml syringe, tissues were manually disassociated in a culture plate containing 10 mls of MACs buffer. Cell suspension was filtered through a 70 μM filter with an additional 20 mls of MACs buffer and pelleted at 500g for 5 mins at 4°C. The pellet was treated with 5 mls of RBC lysis buffer (cat. # 00–4333-57, eBioscience) for 5 mins at room temperature. Lysis was quenched with 30 mls of MACs buffer and the cell suspension was filtered through a 70 μM filter and a 40 μM filter, then pelleted using the above conditions. Cell count was determined using a Z2 Beckmann Coulter counter. Cells were cultured at 1×10^6 cells/ml in RPMI supplemented with $_L$-glutamine (2 mM), sodium pyruvate (1 mM), penicillin (100 U/ml), streptomycin (0.1 mg/ml), and FCS (10%). Cells were stimulated for 4 hrs with PMA (phorbol 12-myristate 13-acetate; 50 ng/ml), ionomycin (Sigma, 750 ng/ml), brefeldin-A (Sigma, 20 ug/ml), then stained with antibodies against surface markers CD3ε, CD4, CD8a (eBioscience) and Aqua Amine Live/Dead (Invitrogen) for 30 mins. After washing, cells were fixed and permeabilized (cat. #00–8333-56, ebioscience) for 20 mins in the dark and stained with fluorophore-conjugated antibodies against intracellular IL-17A and IFNγ (eBioscience). Following washing, cells were fixed with 1.6% paraformaldehyde and analyzed using an LSR II (Becton Dickinson).

Luminex multiple cytokine/chemokine assay

This assay was performed in the Human Immune Monitoring Center at Stanford University. Mouse 26-plex kits were purchased from Affymetrix and used according to the manufacturer's recommendations with modifications as described below. Briefly, samples were mixed with antibody-linked polystyrene beads on 96-well filter-bottom plates and incubated at room temperature for 2 hr followed by overnight incubation at 4°C. Room temperature incubation steps were performed on an orbital shaker at 500–600 rpm. Plates were vacuum filtered and washed twice with wash buffer, then incubated with biotinylated detection antibody for 2 hr at room temperature. Samples were then filtered and washed twice as above and resuspended in streptavidin-PE. After incubation for 40 minutes at room temperature, two additional vacuum washes were performed, and the samples were resuspended in Reading Buffer. Each sample was measured in duplicate. Plates were read using a Luminex 200 instrument with a lower bound of 100 beads per sample per cytokine.

Cytokine stimulation and phosphoflow cytometry

Splenocytes were cultured for at least 2 hours and stained for viability with Aqua Amine Live/Dead (Invitrogen) for 30 mins. Following washing and resting for 30 minutes, splenocytes were stimulated with IFNα (PBL Interferon Source, 1000 U/ml), IFNγ (Peprotech, 50 ng/ml), IL-4 (Peprotech, 50 ng/ml), IL-12 (Peprotech, 50 ng/ml), IL-21 (Peprotech, 50 ng/ml), or IL-27 (R&E Systems, 50 ng/ml) for 20 minutes at 37°C. Stimulation was halted with 1.6% paraformaldehyde for 10 minutes at room temperature. Following washing with FACS buffer (0.5% Bovine Serum Albumin and 0.09% Sodium Azide in PBS), splenocytes were permeabilized using pre-chilled MeOH for 20 minutes at 4°C. Following washing, cells were stained for 1 hour at room temperature with fluorophore-conjugated surface antibodies: CD3 (17A2) eFuor450, CD4 (RM4–5) Alexa 700, CD8a (53–6.7) PerCP-Cy5.5, CD19 (1D3) PE-Cy7, NKp46 (29A1.4) APC (all surface antibodies were purchased from eBioscience except NKp46, which was purchased from BioLegend) in addition to intracellular antibodies against phospho-proteins Stat1 Y701 (4A)

Alexa 488, Stat3 Y705 (4) Alexa 647, Stat4 pY694 (38) PE, Stat5 Y694 (47) Alexa 488, and Stat6 Y641 (J71–773.58.11) Alexa 647 (BD Biosciences). Following washing, cells were fixed with 1.6% paraformaldehyde and analyzed using an LSR II (Becton Dickinson).

Statistical methods

Microarray data were expressed as mean net fluorescence intensity (MFI) units, representing the mean values from six replicate antigen features on each array. Non-reactive samples were defined as having a maximum normalized IgM or IgG MFI of less than 1,000 for a given antigen. The same methods were applied to Luminex multiple bead based assays. For both, Significance Analysis of Microarrays (SAM)[44] was applied to the dataset (with the MFI value of undetected array features set to 1) using the Wilcoxon signed-rank test statistic to identify antigens or cytokines/chemokines with statistically significant differences in array reactivity between different groups of mice at FDR of 0 ($q<0.001$). Binding reactivity heatmaps were generated using MultiExperiment Viewer (MEV TM4 Microarray Software Suite version 10.2, Dana-Farber Cancer Institute, Boston, MA) using k-nearest neighbor replacement and average linkage using Euclidean distance hierarchical clustering.

For ELISA, ICS, qPCR, proteinuria and kidney histology data, significant differences between groups were determined by Mann-Whitney test. For phosphoflow data, significant differences between groups were established as FDR <0.05, calculated by the Benjamini-Hochberg method for multiple hypothesis testing correction.

Supplementary Material

Refer to Web version on PubMed Central for supplementary material.

Acknowledgments

The authors thank P. J. Hertzog for *Ifnar2*$^{-/-}$ mice on the BALB/c; J. Dubin for *Stat1*$^{-/-}$ mice on the BALB/c background; and other members of the Utz and Steinman laboratory for technical assistance and meaningful discussions. This work is supported by NHLBI Proteomics Contract, HHSN288201000034C; by Proteomics of Inflammatory Immunity and Pulmonary Arterial Hypertension the Lupus Foundation of America; by Alliance for Lupus Research, 21858; by Stanford Institute for Immunity; by Transplantation and Infection (ITI) Pilot Grant; by FP Grant #261, by the European Union Seventh Framework Programme (FP7/2007–2013) under grant agreement no° [261382]; by NIH #1S10OD0105800A1, and by a gift from the Floren Family Trust to P.J.Utz. P.J. Utz is the recipient of a Donald E. and Delia B. Baxter Foundation Career Development Award. G. Yiu is supported by the Stanford MSTP and T. K. Rausmussen is supported by the Novo Nordisk Foundation, The Danish Rheumatoid Association, The Graduate School of Health, and Aarhus University (All grants are unrestricted).

REFERENCES

1. Xiong W, Lahita RG. Pragmatic approaches to therapy for systemic lupus erythematosus. Nat. Rev. Rheumatol. 2013 advance online publication.
2. Ledford H. After half-century’s wait, approval paves path for new lupus drugs. Nat. Med. 2011; 17:400. [PubMed: 21475219]
3. Rönnblom LE, Alm GV, Oberg K. Autoimmune phenomena in patients with malignant carcinoid tumors during interferon-alpha treatment. Acta Oncol. Stockh. Swed. 1991; 30:537–540.
4. Baechler EC, et al. Interferon-inducible gene expression signature in peripheral blood cells of patients with severe lupus. Proc. Natl. Acad. Sci. U. S. A. 2003; 100:2610–2615. [PubMed: 12604793]

5. Lyons PA, et al. Novel expression signatures identified by transcriptional analysis of separated leucocyte subsets in systemic lupus erythematosus and vasculitis. Ann. Rheum. Dis. 2010; 69:1208–1213. [PubMed: 19815495]
6. Bauer JW, et al. Elevated Serum Levels of Interferon-Regulated Chemokines Are Biomarkers for Active Human Systemic Lupus Erythematosus. PLoS Med. 2006; 3:e491. [PubMed: 17177599]
7. Lu Q, Shen N, Li XM, Chen SL. Genomic view of IFN-α response in pre-autoimmune NZB/W and MRL/lpr mice. Genes Immun. 2007; 8:590–603. [PubMed: 17728792]
8. Santiago-Raber M-L, et al. Type-I Interferon Receptor Deficiency Reduces Lupuslike Disease in NZB Mice. J. Exp. Med. 2003; 197:777–788. [PubMed: 12642605]
9. Braun D, Geraldes P, Demengeot J. Type I Interferon controls the onset and severity of autoimmune manifestations in lpr mice. J. Autoimmun. 2003; 20:15–25. [PubMed: 12604309]
10. Hron JD, Peng SL. Type I IFN Protects Against Murine Lupus. J. Immunol. 2004; 173:2134–2142. [PubMed: 15265950]
11. Thibault DL, et al. IRF9 and STAT1 are required for IgG autoantibody production and B cell expression of TLR7 in mice. J. Clin. Invest. 2008; 118:1417–1426. [PubMed: 18340381]
12. Thibault DL, et al. Type I interferon receptor controls B-cell expression of nucleic acid-sensing Toll-like receptors and autoantibody production in a murine model of lupus. Arthritis Res. Ther. 2009; 11:R112. [PubMed: 19624844]
13. Rosner S, et al. A multicenter study of outcome in systemic lupus erythematosus. II. Causes of death. Arthritis Rheum. 1982; 25:612–617. [PubMed: 7046757]
14. Ward MM, Pyun E, Studenski S. Causes of death in systemic lupus erythematosus. Long-term followup of an inception cohort. Arthritis Rheum. 1995; 38:1492–1499. [PubMed: 7575699]
15. Theofilopoulos AN, Dixon FJ. Murine models of systemic lupus erythematosus. Adv. Immunol. 1985; 37:269–390. [PubMed: 3890479]
16. Ishida H, et al. Continuous administration of anti-interleukin 10 antibodies delays onset of autoimmunity in NZB/W F1 mice. J. Exp. Med. 1994; 179:305–310. [PubMed: 8270873]
17. Viallard JF, et al. Th1 (IL-2, interferon-gamma (IFN-gamma)) and Th2 (IL-10, IL-4) cytokine production by peripheral blood mononuclear cells (PBMC) from patients with systemic lupus erythematosus (SLE). Clin. Exp. Immunol. 1999; 115:189–195. [PubMed: 9933441]
18. Cross JT, Benton HP. The roles of interleukin-6 and interleukin-10 in B cell hyperactivity in systemic lupus erythematosus. Inflamm. Res. Off. J. Eur. Histamine Res. Soc. Al. 1999; 48:255–261.
19. Leonard WJ, O'Shea JJ. Jaks and STATs: biological implications. Annu. Rev. Immunol. 1998; 16:293–322. [PubMed: 9597132]
20. Hsieh C, et al. Predicting outcomes of lupus nephritis with tubulointerstitial inflammation and scarring. Arthritis Care Res. 2011; 63:865–874.
21. Winfield JB, Faiferman I, Koffler D. Avidity of anti-DNA antibodies in serum and IgG glomerular eluates from patients with systemic lupus erythematosus. Association of high avidity antinative DNA antibody with glomerulonephritis. J. Clin. Invest. 1977; 59:90–96. [PubMed: 299748]
22. Pankewycz OG, Migliorini P, Madaio MP. Polyreactive autoantibodies are nephritogenic in murine lupus nephritis. J. Immunol. 1987; 139:3287–3294. [PubMed: 3500215]
23. Koga T, et al. KN-93, an inhibitor of calcium/calmodulin-dependent protein kinase IV, promotes generation and function of Foxp3(+) regulatory T cells in MRL/lpr mice. Autoimmunity. 2014:1–6. [PubMed: 24245950]
24. Kim H-R, et al. CD4+CD25+ regulatory T cells from MRL/lpr mice were functionally more active in vitro but did not prevent spontaneous as well as adriamycin-induced nephropathy in vivo. Rheumatology. 2012; 51:1357–1367. [PubMed: 22513147]
25. Hou L-F, et al. Oral administration of artemisinin analog SM934 ameliorates lupus syndromes in MRL/lpr mice by inhibiting Th1 and Th17 cell responses. Arthritis Rheum. 2011; 63:2445–2455. [PubMed: 21484768]
26. Deng G-M, Liu L, Bahjat FR, Pine PR, Tsokos GC. Suppression of skin and kidney disease by inhibition of spleen tyrosine kinase in lupus-prone mice. Arthritis Rheum. 2010; 62:2086–2092. [PubMed: 20222110]

27. Austin HA 3rd, Muenz LR, Joyce KM, Antonovych TT, Balow JE. Diffuse proliferative lupus nephritis: identification of specific pathologic features affecting renal outcome. Kidney Int. 1984; 25:689–695. [PubMed: 6482173]
28. Steinmetz OM, et al. CXCR3 Mediates Renal Th1 and Th17 Immune Response in Murine Lupus Nephritis. J Immunol. 2009; 183:4693–4704. [PubMed: 19734217]
29. Xing Q, Wang B, Su H, Cui J, Li J. Elevated Th17 cells are accompanied by FoxP3+ Treg cells decrease in patients with lupus nephritis. Rheumatol Int. 2012; 32:949–958. [PubMed: 21243492]
30. Chen D-Y, et al. The potential role of Th17 cells and Th17-related cytokines in the pathogenesis of lupus nephritis. Lupus. 2012; 21:1385–1396. [PubMed: 22892208]
31. Wong CK, et al. Hyperproduction of IL-23 and IL-17 in patients with systemic lupus erythematosus: implications for Th17-mediated inflammation in auto-immunity. Clin. Immunol. Orlando Fla. 2008; 127:385–393.
32. Cheung PFY, Wong CK, Lam CWK. Molecular mechanisms of cytokine and chemokine release from eosinophils activated by IL-17A, IL-17F, and IL-23: implication for Th17 lymphocytes-mediated allergic inflammation. J. Immunol. Baltim. Md 1950. 2008; 180:5625–5635.
33. Dias PM, Banerjee G. The Role of Th17/IL-17 on Eosinophilic Inflammation. J. Autoimmun. 2013; 40:9–20. [PubMed: 22906357]
34. Rahman MS, et al. IL-17A induces eotaxin-1/CC chemokine ligand 11 expression in human airway smooth muscle cells: role of MAPK (Erk1/2, JNK, and p38) pathways. J. Immunol. Baltim. Md 1950. 2006; 177:4064–4071.
35. Yang J, et al. Th17 and natural Treg cell population dynamics in systemic lupus erythematosus. Arthritis Rheum. 2009; 60:1472–1483. [PubMed: 19404966]
36. Kurts C, Panzer U, Anders H-J, Rees AJ. The immune system and kidney disease: basic concepts and clinical implications. Nat. Rev. Immunol. 2013; 13:738–753. [PubMed: 24037418]
37. Price JV, et al. On silico peptide microarrays for high-resolution mapping of antibody epitopes and diverse protein-protein interactions. Nat. Med. 2012; 18:1434–1440. [PubMed: 22902875]
38. Liu CL, et al. Specific post-translational histone modifications of neutrophil extracellular traps as immunogens and potential targets of lupus autoantibodies. Arthritis Res. Ther. 2012; 14:R25. [PubMed: 22300536]
39. Robinson WH, et al. Autoantigen microarrays for multiplex characterization of autoantibody responses. Nat. Med. 2002; 8:295–301. [PubMed: 11875502]
40. Balboni I, et al. Multiplexed protein array platforms for analysis of autoimmune diseases. Annu. Rev. Immunol. 2006; 24:391–418. [PubMed: 16551254]
41. Price JV, et al. Protein microarray analysis reveals BAFF-binding autoantibodies in systemic lupus erythematosus. J. Clin. Invest. 2013; 123:5135–5145. [PubMed: 24270423]
42. Zhang B, et al. An integrated peptide-antigen microarray on plasmonic gold films for sensitive human antibody profiling. PloS One. 2013; 8:e71043. [PubMed: 23923050]
43. Sekine H, et al. Role of MHC-Linked Genes in Autoantigen Selection and Renal Disease in a Murine Model of Systemic Lupus Erythematosus. J. Immunol. 2006; 177:7423–7434. [PubMed: 17082662]
44. Tusher VG, Tibshirani R, Chu G. Significance analysis of microarrays applied to the ionizing radiation response. Proc. Natl. Acad. Sci. U. S. A. 2001; 98:5116–5121. [PubMed: 11309499]
45. Cerutti A, Qiao X, He B. Plasmacytoid dendritic cells and the regulation of immunoglobulin heavy chain class switching. Immunol. Cell Biol. 2005; 83:554–562. [PubMed: 16174107]
46. Lee BL, et al. UNC93B1 mediates differential trafficking of endosomal TLRs. eLife. 2013; 2:e00291. [PubMed: 23426999]
47. Papin JA, Palsson BO. The JAK-STAT Signaling Network in the Human B-Cell: An Extreme Signaling Pathway Analysis. Biophys. J. 2004; 87:37–46. [PubMed: 15240442]
48. Lin J-X, et al. The role of shared receptor motifs and common stat proteins in the generation of cytokine pleiotropy and redundancy by IL-2, IL-4, IL-7, IL-13, and IL-15. Immunity. 1995; 2:331–339. [PubMed: 7719938]

49. Hale MB, Krutzik PO, Samra SS, Crane JM, Nolan GP. Stage Dependent Aberrant Regulation of Cytokine-STAT Signaling in Murine Systemic Lupus Erythematosus. PLoS ONE. 2009; 4:e6756. [PubMed: 19707593]
50. Huang X, Guo Y, Bao C, Shen N. Multidimensional Single Cell Based STAT Phosphorylation Profiling Identifies a Novel Biosignature for Evaluation of Systemic Lupus Erythematosus Activity. PLoS ONE. 2011; 6:e21671. [PubMed: 21799742]
51. Lan Y, Luo B, Wang J-L, Jiang Y-W, Wei Y-S. The association of interleukin-21 polymorphisms with interleukin-21 serum levels and risk of systemic lupus erythematosus. Gene. 2014; 538:94–98. [PubMed: 24434811]
52. Yang X, et al. T follicular helper cells mediate expansion of regulatory B cells via IL-21 in Lupus-prone MRL/lpr mice. PloS One. 2013; 8:e62855. [PubMed: 23638156]
53. Rankin AL, et al. IL-21 receptor is required for the systemic accumulation of activated B and T lymphocytes in MRL/MpJ-Fas(lpr/lpr)/J mice. J. Immunol. Baltim. Md 1950. 2012; 188:1656–1667.
54. Basu R, Hatton RD, Weaver CT. The Th17 family: flexibility follows function. Immunol. Rev. 2013; 252:89–103. [PubMed: 23405897]
55. Trinchieri G. Interleukin-12: a cytokine produced by antigen-presenting cells with immunoregulatory functions in the generation of T-helper cells type 1 and cytotoxic lymphocytes. Blood. 1994; 84:4008–4027. [PubMed: 7994020]
56. Park MH, D'Agati V, Appel GB, Pirani CL. Tubulointerstitial disease in lupus nephritis: relationship to immune deposits, interstitial inflammation, glomerular changes, renal function, and prognosis. Nephron. 1986; 44:309–319. [PubMed: 3540691]
57. Wehrmann M, et al. Long-term prognosis of focal sclerosing glomerulonephritis. An analysis of 250 cases with particular regard to tubulointerstitial changes. Clin. Nephrol. 1990; 33:115–122. [PubMed: 2323110]
58. Doreau A, et al. Interleukin 17 acts in synergy with B cell-activating factor to influence B cell biology and the pathophysiology of systemic lupus erythematosus. Nat Immunol. 2009; 10:778–785. [PubMed: 19483719]
59. Dong G, et al. IL-17 induces autoantibody overproduction and peripheral blood mononuclear cell overexpression of IL-6 in lupus nephritis patients. Chin. Med. J. (Engl.). 2003; 116:543–548. [PubMed: 12875719]
60. Bettelli E, Oukka M, Kuchroo VK. TH-17 cells in the circle of immunity and autoimmunity. Nat. Immunol. 2007; 8:345–350. [PubMed: 17375096]
61. Chen D-Y, et al. The potential role of Th17 cells and Th17-related cytokines in the pathogenesis of lupus nephritis. Lupus. 2012; 21:1385–1396. [PubMed: 22892208]
62. Wong CK, Ho CY, Li EK, Lam CW. Elevation of proinflammatory cytokine (IL-18, IL-17, IL-12) and Th2 cytokine (IL-4) concentrations in patients with systemic lupus erythematosus. Lupus. 2000; 9:589–593. [PubMed: 11035433]
63. Crispín JC, et al. Expanded Double Negative T Cells in Patients with Systemic Lupus Erythematosus Produce IL-17 and Infiltrate the Kidneys. J. Immunol. 2008; 181:8761–8766. [PubMed: 19050297]
64. Fan X, Wüthrich RP. Upregulation of lymphoid and renal interferon-gamma mRNA in autoimmune MRL-Fas(lpr) mice with lupus nephritis. Inflammation. 1997; 21:105–112. [PubMed: 9179626]
65. Liu J, et al. Genomic view of systemic autoimmunity in MRLlpr mice. Genes Immun. 2006; 7:156–168. [PubMed: 16508641]
66. Schwarting A, Wada T, Kinoshita K, Tesch G, Kelley VR. IFN-gamma receptor signaling is essential for the initiation, acceleration, and destruction of autoimmune kidney disease in MRL-Fas(lpr) mice. J. Immunol. Baltim. Md 1950. 1998; 161:494–503.
67. Valdar W, et al. Genetic and Environmental Effects on Complex Traits in Mice. Genetics. 2006; 174:959–984. [PubMed: 16888333]
68. Klempt M, et al. Genotype-specific environmental impact on the variance of blood values in inbred and F1 hybrid mice. Mamm. Genome Off. J. Int. Mamm. Genome Soc. 2006; 17:93–102.
69. Schnell MA, Hardy C, Hawley M, Propert KJ, Wilson JM. Effect of blood collection technique in mice on clinical pathology parameters. Hum. Gene Ther. 2002; 13:155–161. [PubMed: 11779419]

70. Korn T, et al. IL-21 initiates an alternative pathway to induce proinflammatory TH17 cells. Nature. 2007; 448:484–487. [PubMed: 17581588]
71. Yang XO, et al. STAT3 regulates cytokine-mediated generation of inflammatory helper T cells. J. Biol. Chem. 2007; 282:9358–9363. [PubMed: 17277312]
72. Yang X-P, et al. Opposing regulation of the locus encoding IL-17 through direct, reciprocal actions of STAT3 and STAT5. Nat. Immunol. 2011; 12:247–254. [PubMed: 21278738]
73. Bluyssen HA, et al. Combinatorial association and abundance of components of interferon-stimulated gene factor 3 dictate the selectivity of interferon responses. Proc. Natl. Acad. Sci. 1995; 92:5645–5649. [PubMed: 7539922]
74. Matsumoto M, et al. Activation of the transcription factor ISGF3 by interferon-gamma. Biol. Chem. 1999; 380:699–703. [PubMed: 10430035]
75. Hall JC, et al. Precise probes of type II interferon activity define the origin of interferon signatures in target tissues in rheumatic diseases. Proc. Natl. Acad. Sci. 2012; 109:17609–17614. [PubMed: 23045702]
76. Rothlin CV, Ghosh S, Zuniga EI, Oldstone MBA, Lemke G. TAM receptors are pleiotropic inhibitors of the innate immune response. Cell. 2007; 131:1124–1136. [PubMed: 18083102]
77. Baccala R, et al. Anti-IFN-α/β Receptor Antibody Treatment Ameliorates Disease in Lupus-Predisposed Mice. J. Immunol. 2012; 189:5976–5984. [PubMed: 23175700]
78. Mesa RA, Yasothan U, Kirkpatrick P. Ruxolitinib. Nat. Rev. Drug Discov. 2012; 11:103–104. [PubMed: 22293561]
79. Merrill JT, et al. Safety profile and clinical activity of sifalimumab, a fully human anti-interferon α monoclonal antibody, in systemic lupus erythematosus: a phase I, multicentre, double-blind randomised study. Ann. Rheum. Dis. 2011; 70:1905–1913. [PubMed: 21798883]
80. Petri M, et al. Sifalimumab, a human anti-interferon-α monoclonal antibody, in systemic lupus erythematosus: a phase I randomized, controlled, dose-escalation study. Arthritis Rheum. 2013; 65:1011–1021. [PubMed: 23400715]
81. Kalunian K. Efficacy and safety of rontalizumab (anti-interferon alpha) in SLE subjects with restricted immunosuppressant use: results of a randomized, double-blind, placebo-controlled phase 2 study. Arthritis Rheum. 2012; 64:S1111.

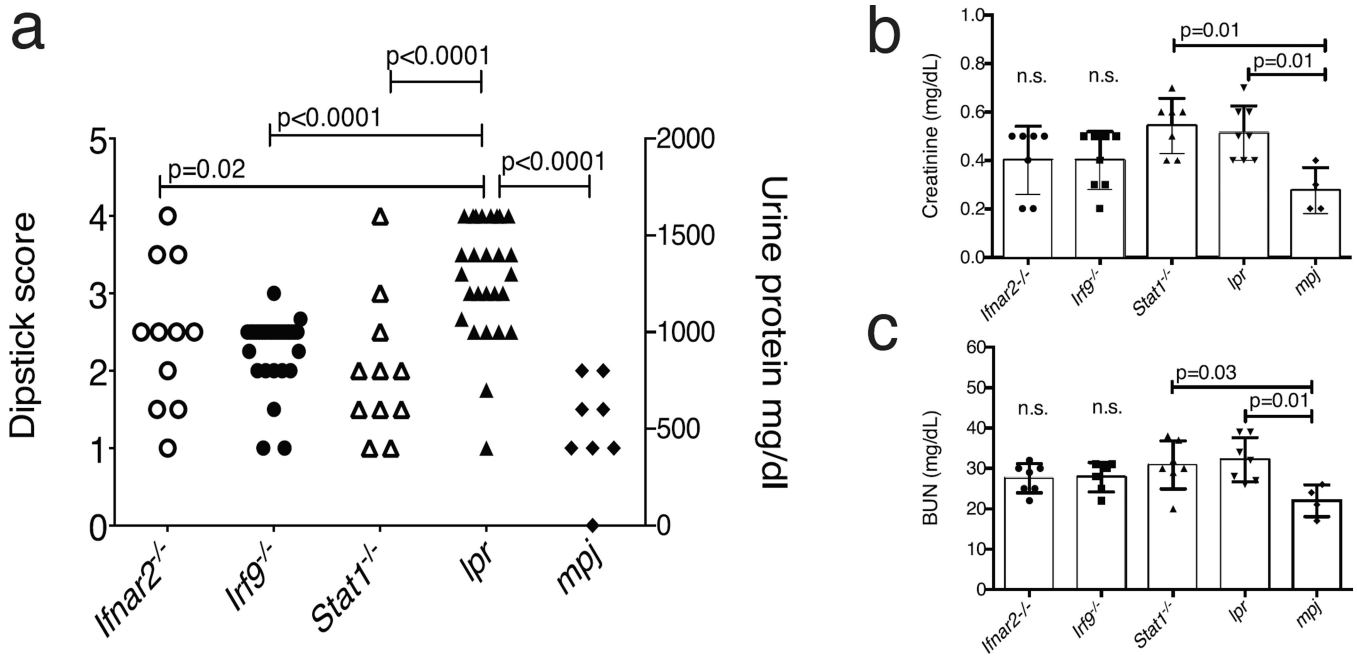

Fig. 1.

Stat1$^{-/-}$ mice exhibit decreased proteinuria but abnormal renal function. **a:** Urine protein levels were determined by Bayer dipsticks in 16-week old mice, *Ifnar2*$^{-/-}$, n= 11; *Irf9*$^{-/-}$, n=30; *Stat1*$^{-/-}$, n=11; *lpr*, n=27; *mpj*, n=8. Serum creatinine **(b)** and Blood Urea Nitrogen (BUN) **(c)** were measured on a clinical chemistry analyzer. Bars represent mean values and error bars represent the standard error of the mean (SEM). P values were determined by Mann-Whitney test, *Ifnar2*$^{-/-}$, n= 7; *Irf9*$^{-/-}$, n=8; *Stat1*$^{-/-}$, n=7; *lpr*, n=8; *mpj*, n=4.

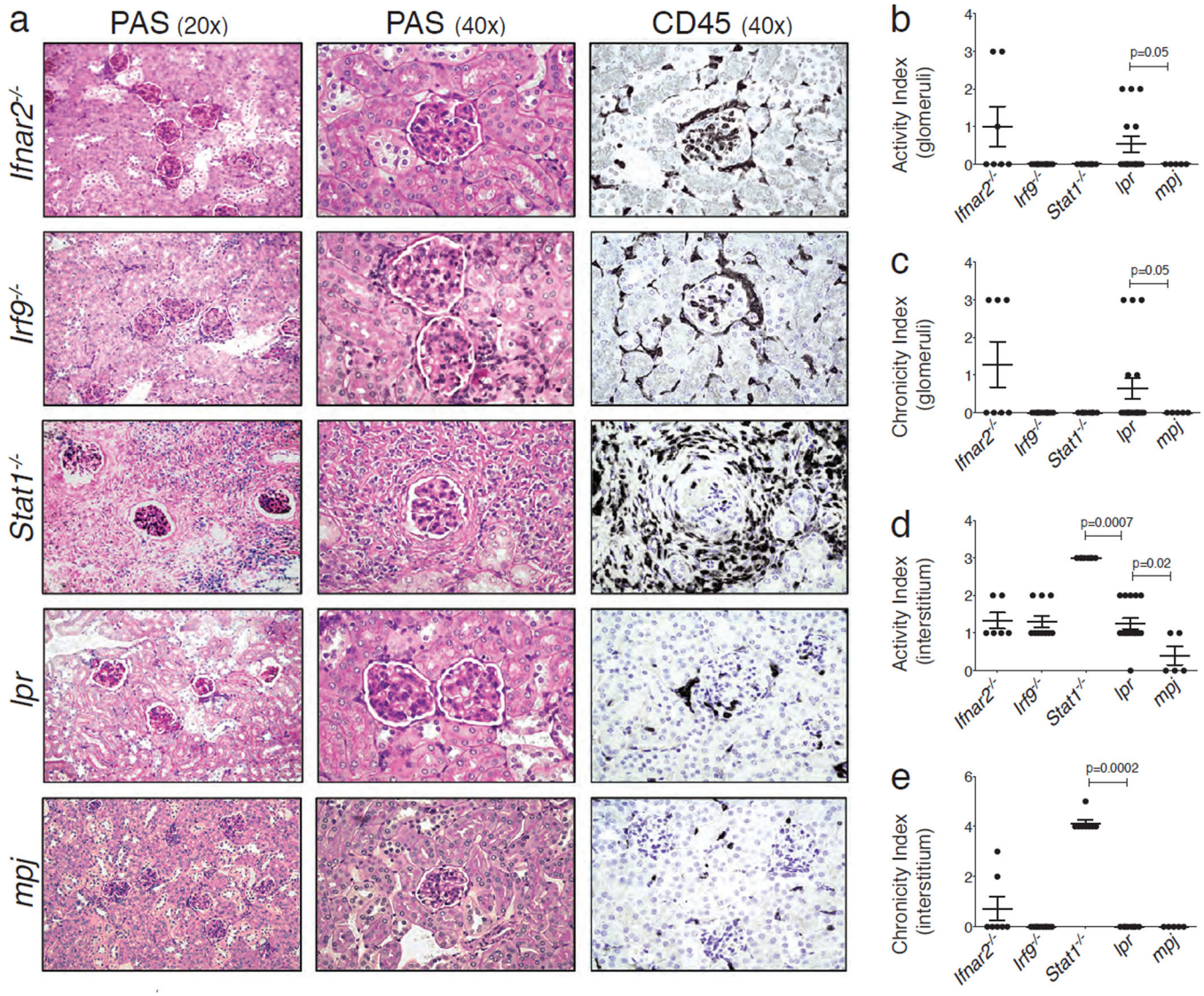

Fig. 2.

Stat1$^{-/-}$ mice display increased interstitial acute and chronic kidney pathology with infiltrating CD45^{+} immune cells. **a: Left**, 5 μm-thick sections were stained with period acid-Schiff (PAS) and imaged at 20X magnification. **Middle**, PAS staining imaged at 40X magnification. **Right**, 5 μm-thick sections were stained for CD45 by immunohistochemistry using 3'Diaminobenzidine (DAB). **b–e:** Kidneys were scored using the NIH activity and chronicity scoring system (Supplemental Table T1). All knockout mice exhibit decreased active (**b**) chronic (**c**) pathology. *Stat1*$^{-/-}$ mice exhibit increased acute (**d**) chronic (**e**) interstitial pathology. *Ifnar2*$^{-/-}$, n= 7; *Irf9*$^{-/-}$, n=10; *Stat1*$^{-/-}$, n=8; *lpr*, n=11; *mpj*=5. Bars represent mean values and error bars represent the standard error of the mean (SEM). P values were determined by Mann-Whitney test.

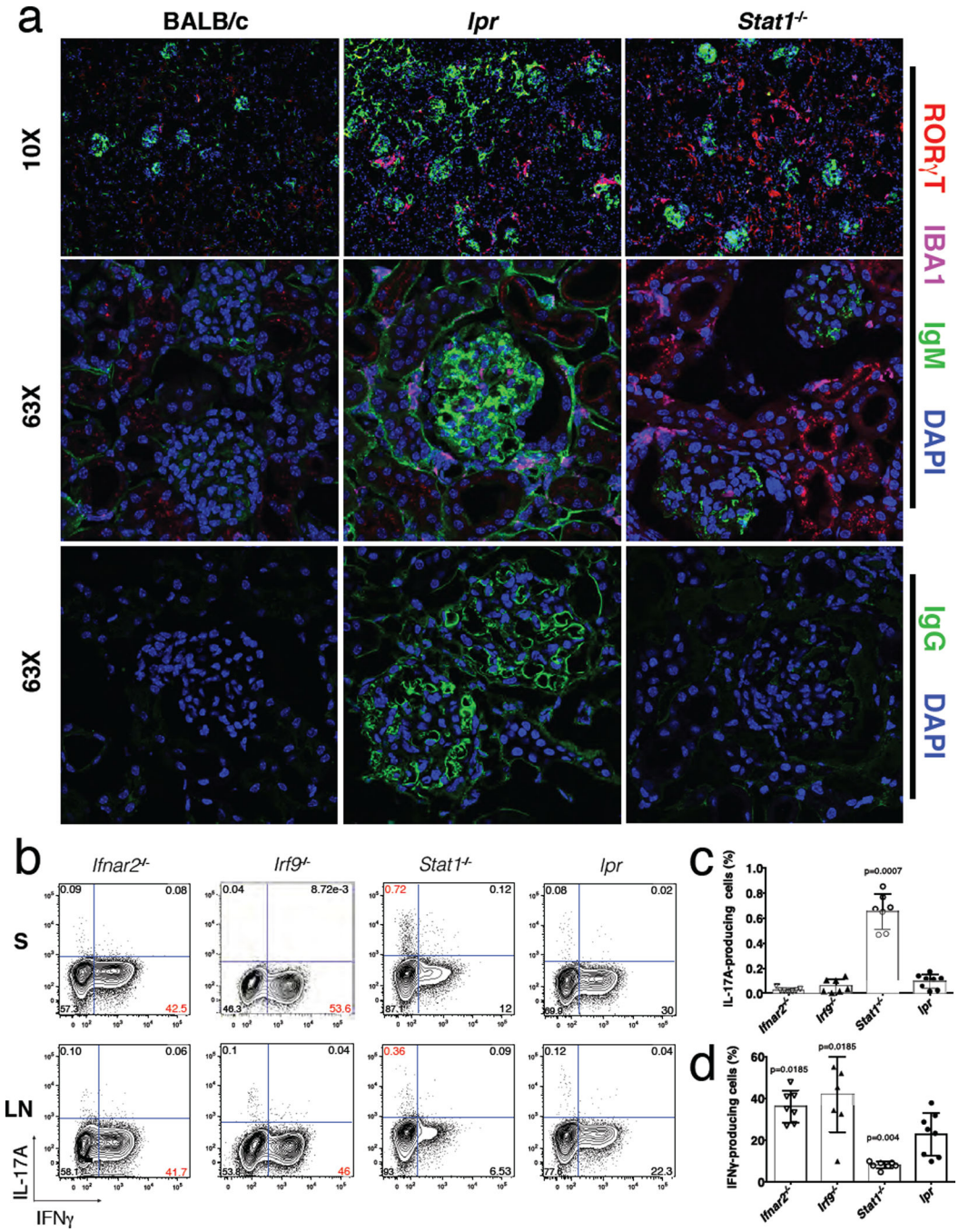

Fig. 3.

Mice genetically-deficient for IFN-signaling components display differential accumulation of cells expressing RORγT^{+} in the kidney interstitium and IL-17A/IFNγ in secondary lymphoid organs. **a:** 7 μm-thick frozen sections were stained for RORγT (red), IBA1 (magenta), IgM (green) and DAPI (blue). *Stat1*$^{-/-}$ mice exhibit increased Th17 and macrophage infiltration in the interstitium. **b:** Intracellular staining of spleen **(top panels)** or lymph node **(bottom panels)** for IFNγ (x-axis) and IL-17A (y-axis) show increased frequencies of IL-17A producing CD4^{+} T cells in *Stat1*$^{-/-}$ mice and increased frequencies of

IFNγ-producing $CD4^+$ T cells in *Irf9*$^{-/-}$ and *Ifnar2*$^{-/-}$ mice. Data for BALB/c mice with and without STAT1 are shown in Supplemental Fig. S3. **c/d:** Graphical representation of flow cytometry data from spleen. *Ifnar2*$^{-/-}$, n=7; *Irf9*$^{-/-}$, n=7; *Stat1*$^{-/-}$, n=7; *lpr*, n=8. P values were determined by Mann-Whitney test. Error bars represent SEM.

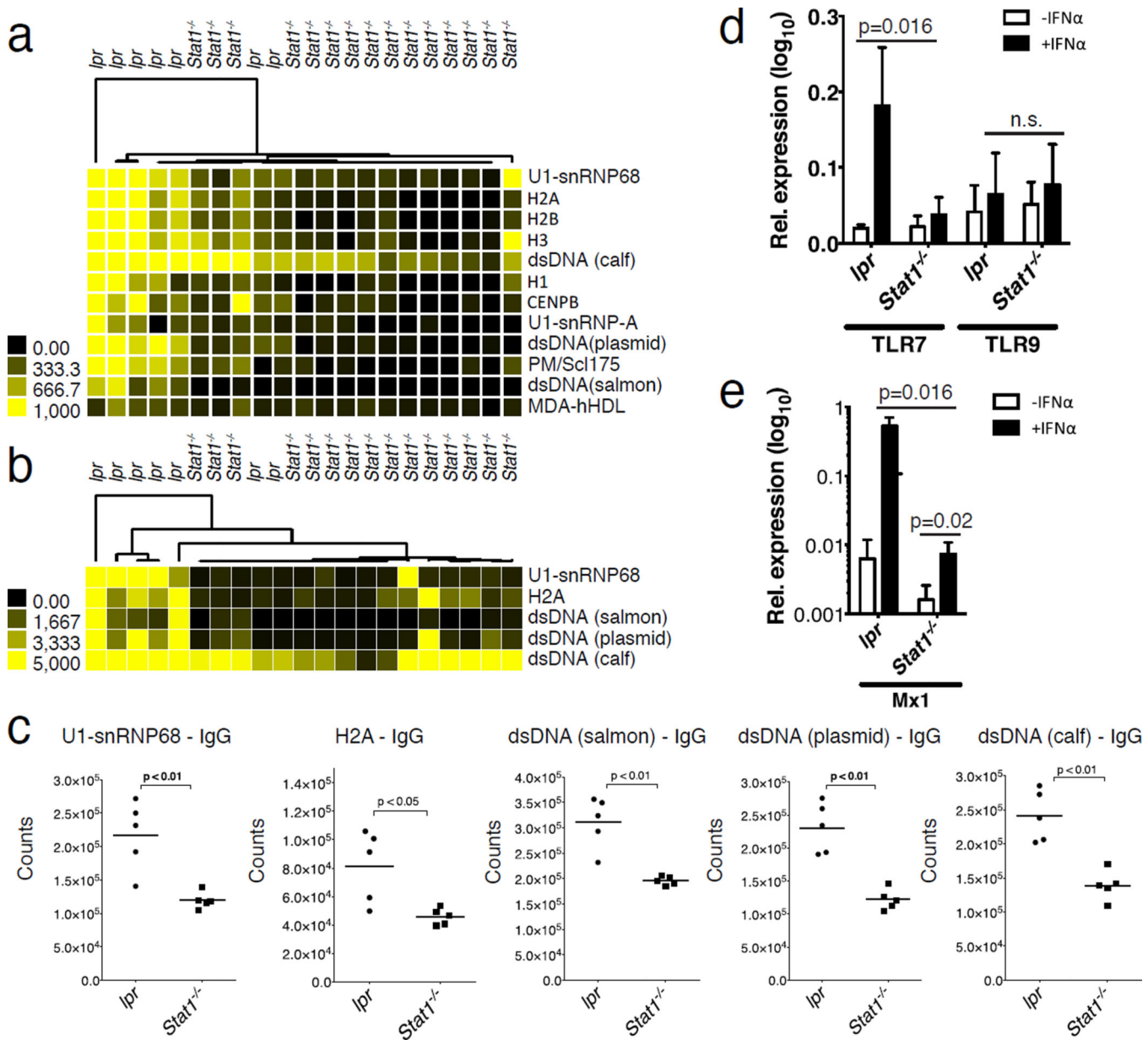

Fig. 4.

Stat1$^{-/-}$ mice exhibit decreased autoantibody production against SLE-associated antigens. Individual autoantigen arrays containing over 600 features and 100 antigens were incubated with serum obtained from *lpr*, *Ifnar2*$^{-/-}$, *Stat1*$^{-/-}$, and *Irf9*$^{-/-}$ mice. The SAM algorithm was used to determine antigen features with statistically significant differences in reactivity between sera derived from either *lpr*, *Stat1*$^{-/-}$, *Irf9*$^{-/-}$ or *Ifnar2*$^{-/-}$ mice. Hierarchical clustering of samples based on reactivity to antigens with statistically significant differences is displayed as a heatmap and dendrogram. Sera from *Stat1*$^{-/-}$ and *lpr* mice were used to probe autoantigen arrays and detected with anti-IgM (**Fig. 4a**) and anti-IgG secondary (**Fig. 4b**) antibodies. The same methods employed in **Fig. 4a and 4b** were employed with sera from *Irf9*$^{-/-}$ and *lpr* mice (Supplementary Figure S3). SAM did not identify any features

with statistically significant differences between *Ifnar2*$^{-/-}$ and *lpr* mice. **c:** Confirmation of SAM-identified IgG (**Fig. 4c**) and IgM (Supplemental Fig. S5) autoantibodies performed by ELISA. Data represent time resolved fluorescence for serum samples obtained from individual mice. Horizontal bars represent mean counts for each group. *P* values were determined by Mann-Whitney test. *lpr*, n=5, *Stat1*$^{-/-}$, n=5. **d/e:** *Stat1*$^{-/-}$ or *lpr* B cells were stimulated with or without IFNα for 4 hours and relative expression of Mx1, TLR7 and TLR9 was measured. P values were determined by Mann-Whitney test.

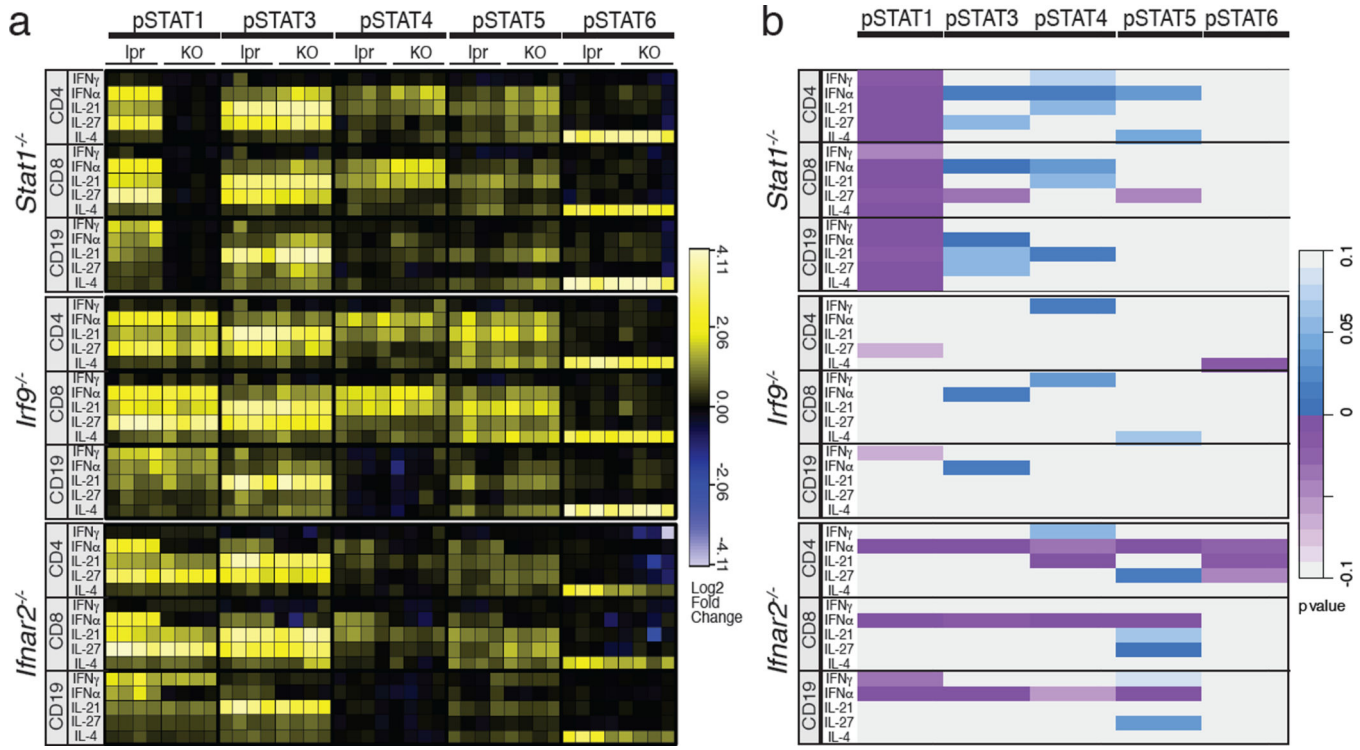

Fig. 5.

Targeted deletion of genes encoding IFN-I/II signaling proteins results in shunting of STAT phosphorylation downstream of cytokine stimulation. Splenocytes from *Stat1*$^{-/-}$, *Irf9*$^{-/-}$, *Ifnar2*$^{-/-}$, and *lpr* mice were stimulated with IFNα, IFNγ, IL-4, IL-21, or IL-27. Phosphorylation of STATs 1, 3, 4, 5, 6 in CD4^{+} T cells, CD8^{+} T cells, or CD19^{+} B cells, was measured by phosphoflow cytometry. **a:** Fold change of cytokine stimulated over unstimulated condition for individual knockout or *lpr* mice, shown in heatmap form (data were Log2 transformed). Yellow and blue represent increases or decreases in phosphorylation levels compared to baseline, respectively. Four representative mice were selected per group. **b:** Phosphorylation of individual STAT proteins downstream of an individual cytokine in one cell subset was compared to corresponding data in *lpr* mice. Uncorrected p-values determined by Mann-Whitney test are represented in heatmap format. Direction of increased or decreased STAT phosphorylation in comparison to *lpr* is represented by blue and purple, respectively. *Ifnar2*$^{-/-}$, n=6; *Irf9*$^{-/-}$, n=4; *Stat1*$^{-/-}$, n=6; *lpr*, n=6. Bar charts of data indicating significance of fold change are presented in Supplemental Fig. S7–S9.